J. Iron Steel Res. Int. (2020) 27:33–41
https://doi.org/10.1007/s42243-018-0218-9

ORIGINAL PAPER

Effect of SiO_2 substitution with Al_2O_3 during high-Al TRIP steel casting on crystallization and structure of low-basicity CaO–SiO_2-based mold flux

Ding-li Zheng[1] · Cheng-bin Shi[1] · Zhi-jun Li[2] · Jing Li[1] · Jung-wook Cho[3]

Received: 30 September 2018 / Revised: 18 December 2018 / Accepted: 19 December 2018 / Published online: 4 January 2019

Abstract
The crystallization and structure of non-conventional lime–silica-based mold fluxes after undergoing slag–steel interaction in casting high-Al transformation induced plasticity (TRIP) steel were studied. The results showed that the crystallization temperatures of the mold fluxes decreased with decreasing the SiO_2/Al_2O_3 ratio, and CaO/MnO_2 ratio had an opposite effect on the crystallization temperatures. The crystalline phases precipitated in the mold flux were $Ca_4Si_2O_7F_2$ and $NaAlSiO_4$. Decreasing SiO_2/Al_2O_3 ratio and increasing CaO/MnO_2 ratio in the mold fluxes have no influence on the types of crystalline phases. The dominant crystalline phase precipitated in each mold flux was $Ca_4Si_2O_7F_2$ with dendritic morphology, except for part of that with globular morphology in the mold flux without MnO_2 addition. $NaAlSiO_4$ crystals are distributed in the space among $Ca_4Si_2O_7F_2$ crystals. The size of $Ca_4Si_2O_7F_2$ crystals in the slag with higher SiO_2/Al_2O_3 ratio is smaller, which is attributed to the polymerization degree of the mold flux with increasing SiO_2/Al_2O_3 ratio. [SiO_4]-tetrahedral, [AlO_4]-tetrahedral and T–O–T bending (T denotes Si or Al) depolymerized gradually with decreasing SiO_2/Al_2O_3 ratio, and an opposite trend was observed for the case with increasing CaO/MnO_2 ratio. The polymerization degree of the mold fluxes decreased, which would result in the decrease in the viscosity of the mold fluxes.

Keywords Mold flux · Crystallization · Structure · Continuous casting · High-Al steel

1 Introduction

The reduction of SiO_2 and accumulation of Al_2O_3 in lime–silica-based mold flux have always been one of the extremely serious issues in continuous casting of high-Al steels because of the steel/slag chemical interaction. Conventional lime–silica-based mold fluxes brought about poor castability and slab surface quality when casting high-aluminum steels due to continuous reduction of SiO_2 and accumulation of Al_2O_3 in the mold flux. The change in the chemistries of mold fluxes led to the variation in viscosity, flux consumption, poor castability and surface quality during continuous casting of high-aluminum steels [1–6].

In recent years, considerable attempts have been made to develop CaO–Al_2O_3-based mold fluxes as substitutes for conventional lime–silica-based mold fluxes for casting high-Al steels [5–12]. The production trials of high-Al transformation induced plasticity (TRIP) steel casting showed that the steel/slag interaction was markedly reduced and the as-cast slab quality was obviously improved when using developed lime–alumina-based mold fluxes by Blazek et al. [2] compared with lime–silica-based mold flux. Cho et al. [6] reported that the lubrication and mold heat transfer in casting 1.45 mass% Al TRIP steel and surface quality of slab were improved by using the developed lime–alumina-based mold fluxes. Fu et al. [7] reported that the crystalline phases changed from CaF_2 and $LiAlO_2$ to $Ca_3Al_2O_6$ and CaO in the designed CaO–Al_2O_3-based mold fluxes with the increase in CaO/Al_2O_3 ratio.

✉ Cheng-bin Shi
chengbin.shi@ustb.edu.cn

[1] State Key Laboratory of Advanced Metallurgy, University of Science and Technology Beijing, Beijing 100083, China

[2] Division of Steelmaking, Shougang Qian'an Iron and Steel Co., Ltd., Qian'an 064404, Hebei, China

[3] Graduate Institute of Ferrous Technology, Pohang University of Science and Technology, Pohang 790-784, Republic of Korea

Wang et al. [8, 9] clarified the effect of B_2O_3, BaO, Li_2O and Na_2O on crystallization behavior of the developed $CaO–Al_2O_3$-based mold fluxes in a series of articles and provided guidance for the optimization and application of the mold fluxes for casting high-Al steels. $CaO–Al_2O_3$-based mold fluxes are still quite needed for the industrial application in casting high-Al steels.

The combination of operational stability and slab surface quality concerns led to the development of non-conventional lime–silica-based mold fluxes with a lower basicity than the conventional lime–silica-based mold fluxes [5, 6]. The mold flux was designed with a low basicity of approximately 0.55, and manganese oxide was added in the non-conventional lime–silica-based mold flux, which in theory was to act as a sacrificial compound to minimize the reaction between aluminum in liquid steel and SiO_2 in the mold flux. The pilot trials of casting high-aluminum TRIP steel using low-basicity $CaO–SiO_2$-based mold flux (AM1 in Ref. [6]) at POSCO showed that the surface had many horizontal and vertical depressions and many surface cracks associated with the depressions, and the surface quality was the worst at the beginning and end of the cast. It is believed to be closely correlated with mold heat transfer behavior and lubrication performance of mold flux, depending largely on the crystallization and viscosity of the mold flux.

Based on the chemical compositions of the spent mold flux when casting high-Al TRIP steel using $CaO–SiO_2$-based mold flux (AM1 in Ref. [6]), the crystallization and structure of the mold flux after undergoing steel/slag interaction during casting were studied. The present study was also undertaken to reveal the crystallization and structure of low-basicity $CaO–SiO_2$-based mold fluxes with varying manganese oxide contents, which was a potential sacrificial compound to minimize the reaction between aluminum in liquid steel and SiO_2 in the mold flux.

2 Experimental

2.1 Sample preparation

According to the chemical composition of the molten slag samples that were obtained every 2 m of casting length in production trails of high-Al TRIP steel casting when using mold flux AM1 in Ref. [6], reagent-grade $CaCO_3$, SiO_2, Al_2O_3, MnO_2, Na_2CO_3, Li_2CO_3 and CaF_2 were used to produce slag samples. $CaCO_3$ powders were calcined at 1050 °C for 10 h in a muffle furnace to produce CaO. The thoroughly mixed powders were pre-melted at 1500 °C for 5 min to homogenize chemical composition and subsequently quenched into ice water to obtain a fully glassy phase. The quenched slag was confirmed to be amorphous according to X-ray diffraction (XRD) identification, as shown in Fig. 1. The ion-selective electrode method was employed to measure the fluorine content in the pre-melted slag. The contents of other components in the slag were analyzed by inductively coupled plasma atomic emission spectroscopy (ICP-AES). The chemical compositions of the studied slag after pre-melting are given in Table 1.

2.2 Differential scanning calorimetry measurement

Differential scanning calorimetry (DSC) measurements using a Netzsch STA449F3 instrument (Netzsch Instrument Inc., Germany) were taken in Ar gas atmosphere at a flow rate at 70 mL/min to investigate the crystallization characteristics of the slags. For each DSC measurement, approximately 50 mg of sample powders was heated at a constant heating rate of 30 °C/min from room temperature up to 1500 °C in a platinum crucible with a diameter of 5 mm and a height of 5 mm and held at this temperature for 1 min to eliminate bubbles and homogenize its chemical composition. Subsequently, the liquid sample was cooled at the cooling rate of 10 °C/min to room temperature.

2.3 Scanning electron microscopy–energy-dispersive X-ray spectrometry and X-ray diffraction analysis

After DSC measurements, the solidified slag was mounted with epoxy resin and polished. Then, a platinum film was sprayed onto the cross section of the polished sample to enhance the sample electric conductivity. The microstructure and crystal compositions of the slag samples were determined by scanning electron microscopy

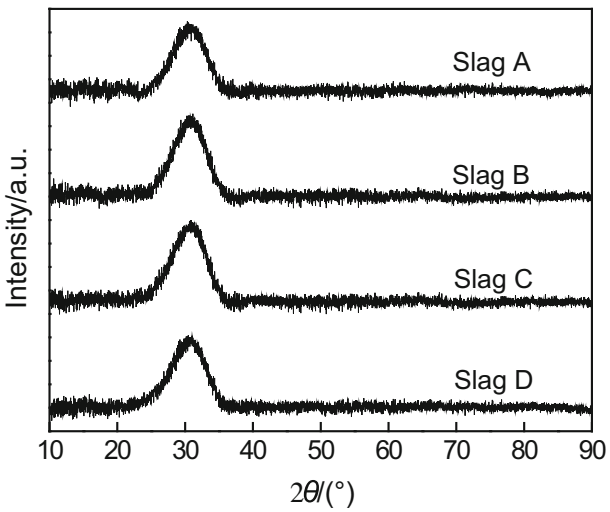

Fig. 1 XRD patterns of as-quenched slag samples

Table 1 Chemical compositions of studied slags after pre-melting (mass%)

Sample No.	CaO	SiO_2	Al_2O_3	MnO_2	Na_2O	F	Li_2O
A	23.6	33.3	11.8	7.2	11.6	10.4	2.2
B	23.7	29.7	15.2	7.2	12.0	10.0	2.2
C	27.5	29.3	15.6	2.9	12.2	10.1	2.3
D	30.5	29.3	15.6	–	12.2	10.1	2.3

(SEM) (FEI Quanta-250; FEI Corporation, Hillsboro, OR) equipped with energy-dispersive X-ray spectrometry (EDS) (XFlash 5030; Bruker, Germany). Because of the small amount of the slag sample after DSC measurements, which is hard to identify the crystalline phase by XRD, approximately 1 g of slag sample was melted in a platinum crucible at 1500 °C for 1 min and subsequently cooled in a muffle furnace at the rate of 10 °C/min to room temperature. The powdery solidified slags were ground and analyzed by XRD with Cu Kα radiation to identify the crystalline phases.

2.4 Fourier transform infrared spectroscopy measurement

The structure of the glassy slag samples was analyzed by Fourier transform infrared (FTIR) spectroscopy. About 2.0 mg of slag powders mixed with 200 mg KBr (reagent grade) was pressed into thin section disk for FTIR measurement. The FTIR measurement was taken using a spectrophotometer equipped with a KBr detector, and the spectra were recorded in the range of 4000–400 cm^{-1}.

3 Results and discussion

3.1 Non-isothermal DSC measurement

The crystallization temperatures and crystal formation in the mold fluxes were determined by DSC. Figure 2 shows the DSC curves of slag samples at the cooling rate of 10 °C/min. The exothermic peak on DSC curve indicates the crystalline phase formation. As shown in Fig. 2, there are two exothermic peaks on DSC curves, indicating the presence of two crystallization events for each slag sample. The peaks on DSC curves are designated as P1 and P2, respectively. The DSC results show that the exothermic peaks on DSC curves shift toward lower temperature with decreasing SiO_2/Al_2O_3 ratio and increasing CaO/MnO_2 ratio.

The onset temperature of the exothermic peaks during continuous cooling can be determined as the crystallization

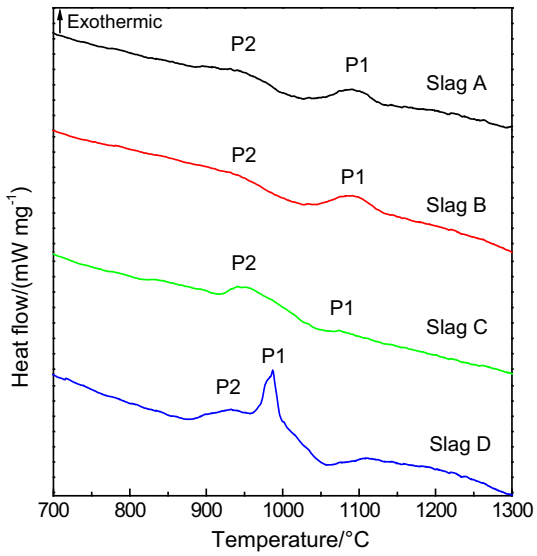

Fig. 2 DSC curves of non-isothermal crystallization of mold fluxes at cooling rate of 10 °C/min

temperature of crystalline phases, at which the crystalline phases start to precipitate during non-isothermal crystallization process [13, 14]. Figure 3 presents the crystallization temperatures of the slag samples at the cooling rate of 10 °C/min. The crystallization temperatures were found to decrease with decreasing SiO_2/Al_2O_3 ratio and increasing CaO/MnO_2 ratio.

The previous pilot trials showed that there were many horizontal and vertical depressions on the slab surface when using low-basicity $CaO–SiO_2$-based mold flux (AM1 in Ref. [6]) for casting high-Al TRIP steel, and many of these depressions contained open cracks [6]. The present study demonstrated that the crystallization temperature of low-basicity $CaO–SiO_2$-based mold fluxes (AM1 in Ref. [6]) decreased during ongoing casting high-Al TRIP steel, and it was much lower than that of developed $CaO–Al_2O_3$-based mold fluxes (as presented in Ref. [10]). The lower

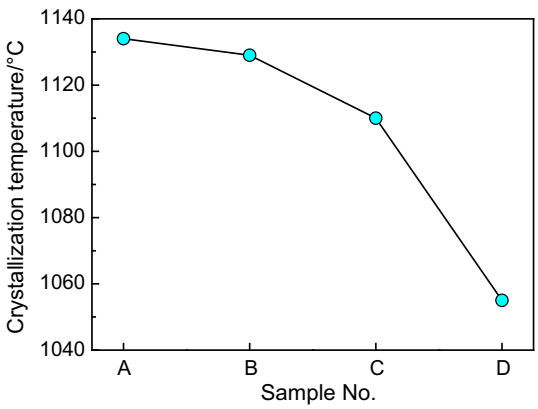

Fig. 3 Change in crystallization temperature in studied mold fluxes at cooling rate of 10 °C/min

crystallization temperature led to a low thermal resistance and excessive mold heat transfer rate, which brought about irregular solidification in the casting mold, consequently resulting in the generation of depressions on the slab surface.

3.2 SEM–EDS observation and XRD identification of crystals in slag

It was determined by DSC measurements that two crystal formation events occurred at the cooling rate of 10 °C/min. XRD analysis was conducted to identify the crystalline phase in the quenched mold fluxes. Figure 4 shows the XRD patterns of the mold fluxes cooling at the rate of 10 °C/min to room temperature. The XRD results suggested that the crystalline phases precipitated in the mold fluxes are $Ca_4Si_2O_7F_2$ crystal and $NaAlSiO_4$ crystal. There are no changes in the types of the crystalline phase in the studied slags during cooling at the rate of 10 °C/min. It indicated that decreasing SiO_2/Al_2O_3 ratio and increasing CaO/MnO_2 ratio had no influence on the types of crystalline phases in the studied mold fluxes at the cooling rate of 10 °C/min.

The crystalline phase in the mold fluxes plays an important role in controlling the horizontal heat transfer in continuous casting process [6, 15]. Accordingly, the crystalline phases in the quenched slags were observed by SEM–EDS, as shown in Figs. 5–12. It was confirmed that two kinds of crystalline phases precipitated in the mold fluxes, which is consistent with the DSC and XRD results.

The morphology of the dominant crystalline phase in each mold flux was dendritic shape, except for part of that with globular morphology in slag D, which was identified as $Ca_4Si_2O_7F_2$ by combining SEM–EDS element mappings results with XRD patterns. Another crystalline phase was confirmed to be $NaAlSiO_4$ in the four slags. The morphology of $NaAlSiO_4$ in slags B and C is rodlike, while it is reticular and faceted in slags A and D, respectively. The $NaAlSiO_4$ crystal is distributed in the space among $Ca_4Si_2O_7F_2$ crystals.

There is a considerable difference in the size of $Ca_4Si_2O_7F_2$ crystal in the mold fluxes. It can be seen that the size of $Ca_4Si_2O_7F_2$ crystal in slag A is obviously smaller than that of other three slags. Crystallization consists of both nucleation and crystal growth processes.

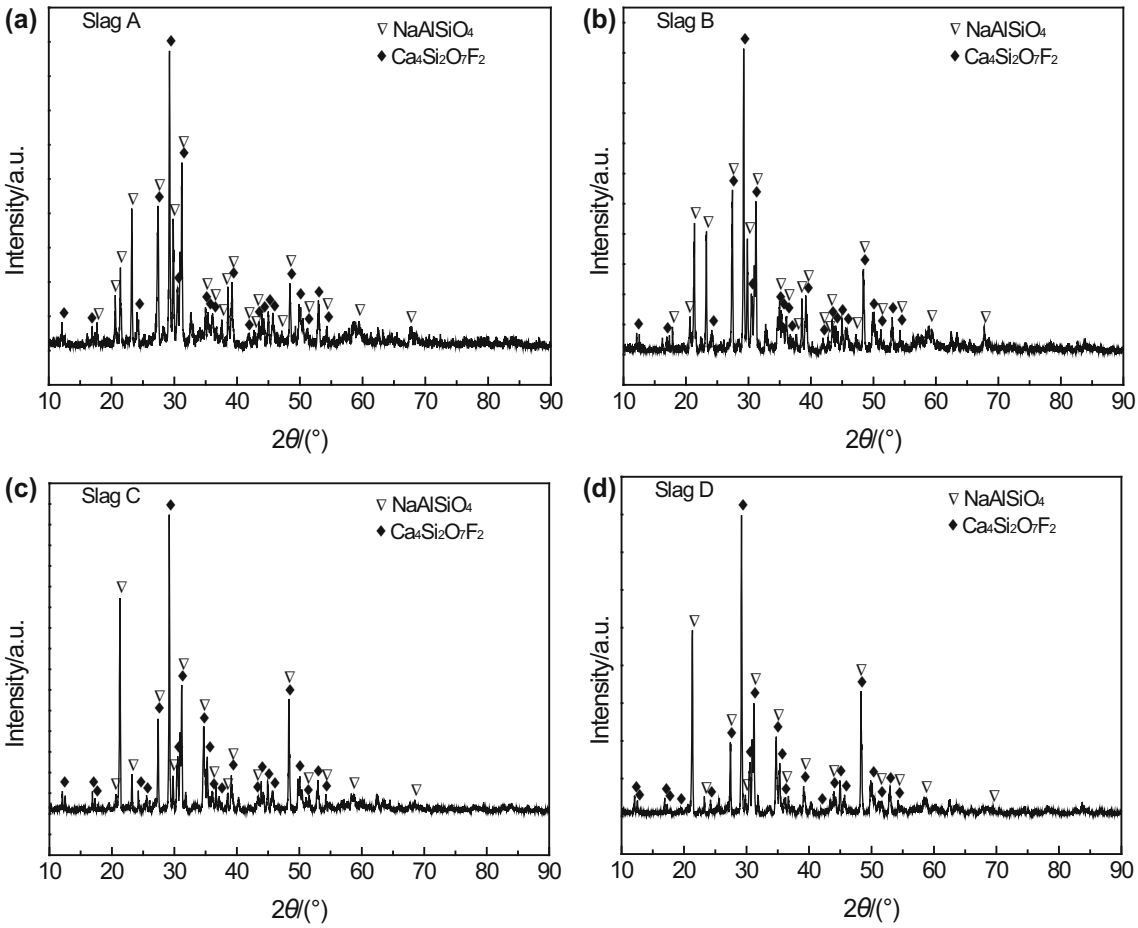

Fig. 4 XRD patterns of mold fluxes quenched at cooling rate of 10 °C/min to room temperature

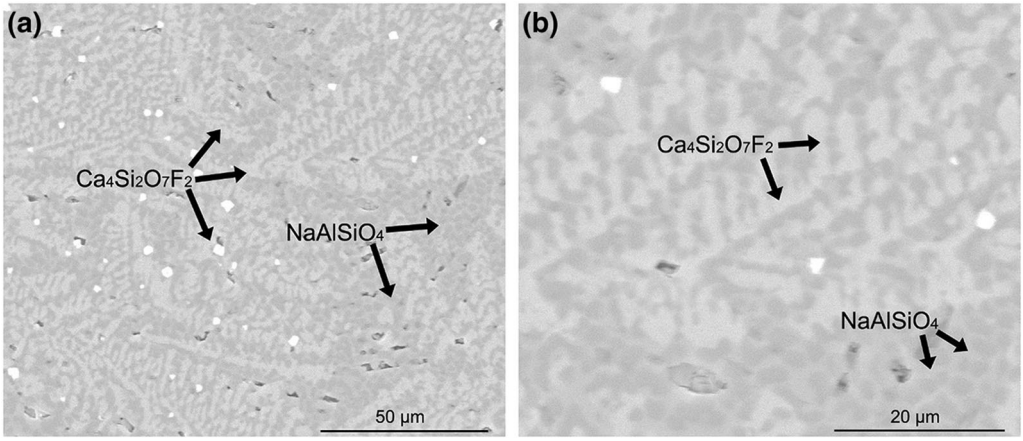

Fig. 5 SEM images of slag A cooled at 10 °C/min

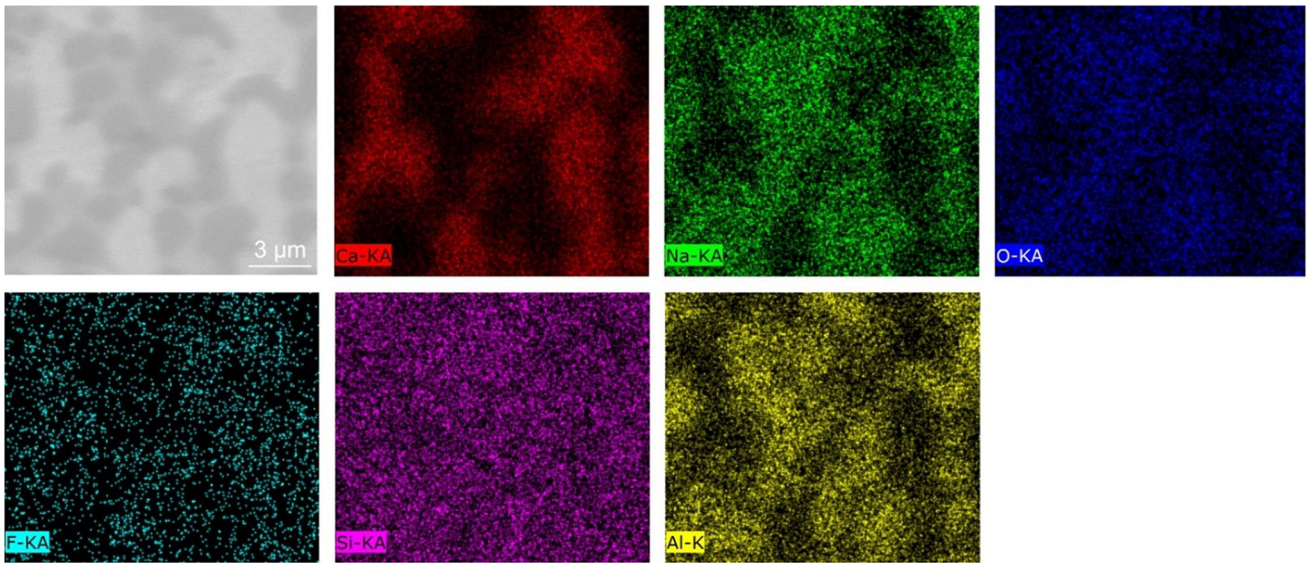

Fig. 6 Element mappings of crystals in slag A cooled at 10 °C/min

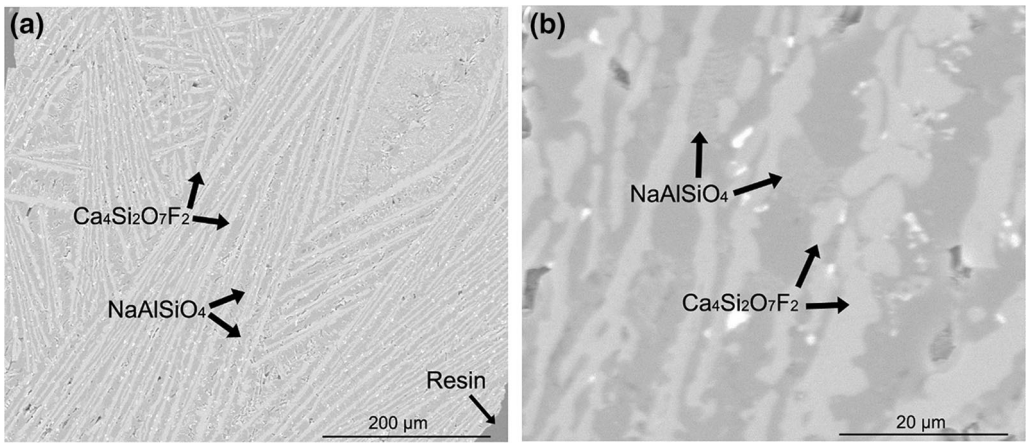

Fig. 7 SEM images of slag B cooled at 10 °C/min

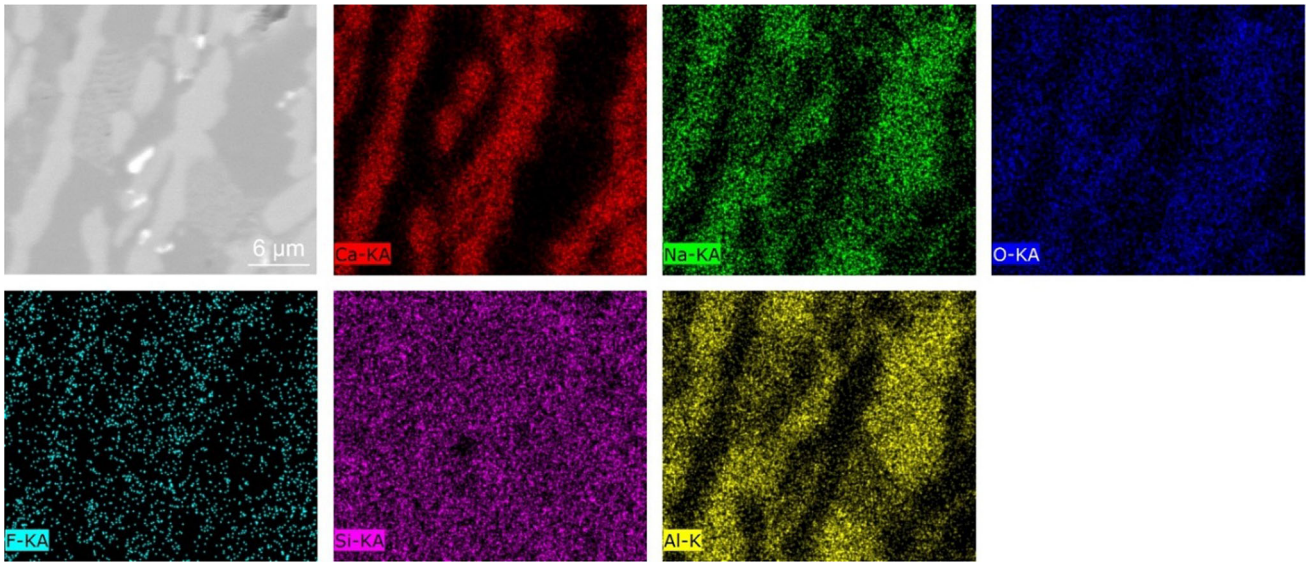

Fig. 8 Element mappings of crystals in slag B cooled at 10 °C/min

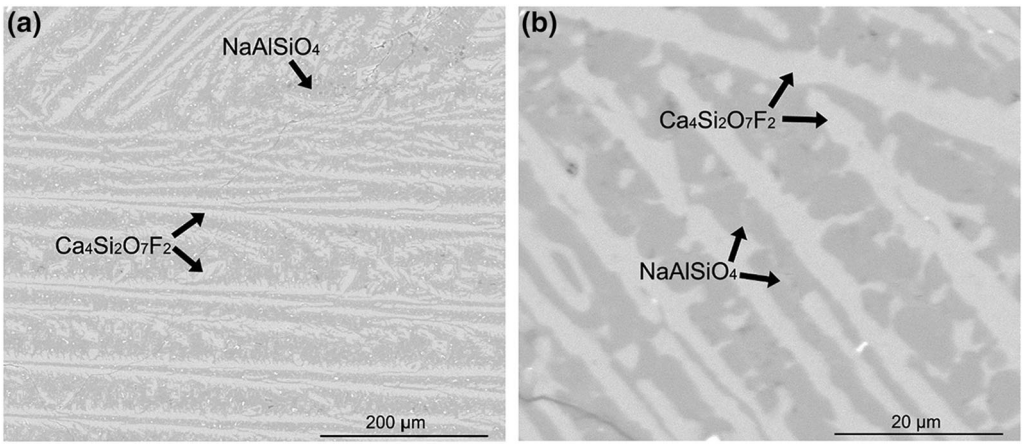

Fig. 9 SEM images of slag C cooled at 10 °C/min

According to the schematic diagram of nucleation and crystal growth rate as a function of temperature reported in previous researches [16, 17], the growth rate is much smaller than the nucleation rate at low crystallization temperature. This is because the obvious increase in the viscosity of slag at low crystallization temperature enhances diffusion resistance of slag components. Therefore, it is difficult for the nucleated particle to grow. The viscosity of the mold flux is correlated with the polymerization degree. The polymerization degree of slag A which has higher SiO_2/Al_2O_3 ratio is evidently higher than that of other three slags, which will be presented in the next section. Therefore, it can be concluded that $Ca_4Si_2O_7F_2$ crystal with the smaller size in slag A is attributed to the higher polymerization degree of slag A.

3.3 Structure analysis using FTIR spectroscopy

The proper viscosity of the mold flux can provide adequate lubrication during continuous casting process. The change in viscosity results from the variation in mold flux structure. Therefore, it is necessary to reveal the effect of SiO_2/Al_2O_3 ratio and CaO/MnO_2 ratio on the structure of the mold flux.

Figure 13 presents the FTIR results of the quenched glassy mold fluxes. It could be observed that the effective spectra ranging from 400 to 1400 cm^{-1} can be divided into three parts: 800–1200 cm^{-1}, 600–800 cm^{-1} and 400–600 cm^{-1}. The assignments of FTIR bands for various structural units are summarized in Table 2.

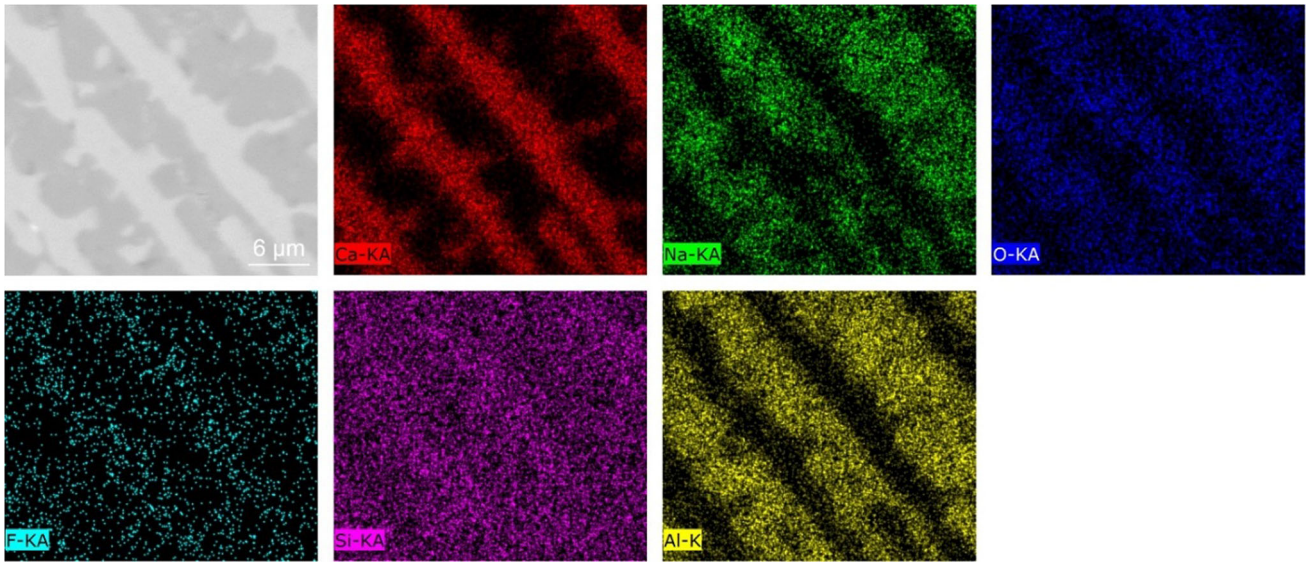

Fig. 10 Element mappings of crystals in slag C cooled at 10 °C/min

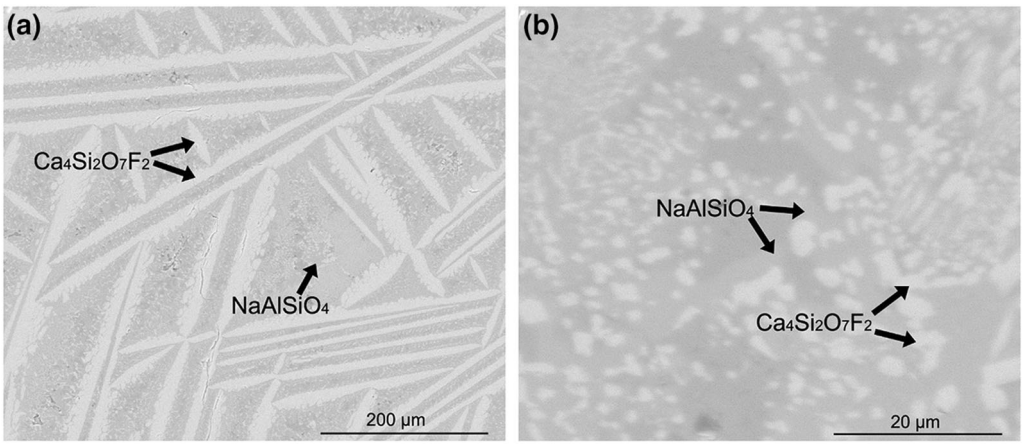

Fig. 11 SEM images of slag D cooled at 10 °C/min

The FTIR band in the region of about 800–1200 cm^{-1} is assigned to $[SiO_4]$-tetrahedral stretching vibration. The major bands at 1200, 1050, 1000–950, 900 and 850 cm^{-1} are associated with Q^4, Q^3, Q^2, Q^1 and Q^0 (the superscript denotes the number of bridging oxygen (BO) per tetrahedrally coordinated silicon), respectively. More BO/Si number at a higher wavenumber means a higher polymerization degree and more complex structure. Figure 13 shows that the center of the region at about 800–1200 cm^{-1} shifts from about 953 to 937 cm^{-1}, indicating that the number of $[SiO_4]$-tetrahedral with less bridging oxygen increased. It suggested that the degree of polymerization of $[SiO_4]$-tetrahedral decreased with decreasing SiO_2/Al_2O_3 ratio and increasing CaO/MnO_2 ratio.

The bands observed at about 600–800 cm^{-1} and 400–600 cm^{-1} are due to $[AlO_4]$-tetrahedral stretching vibration and T–O–T bending vibrations, respectively. Figure 13 shows that the relative intensity of $[AlO_4]$-tetrahedral stretching vibration and T–O–T bending vibrations both became less pronounced gradually, suggesting the depolymerization of T–O–T bending of the slag melts.

Consequently, $[SiO_4]$-tetrahedral, $[AlO_4]$-tetrahedral and T–O–T bending depolymerized gradually with decreasing SiO_2/Al_2O_3 ratio, and a same trend was observed for the case with increasing CaO/MnO_2 ratio. The degree of polymerization of the mold fluxes decreased, which would result in the decrease in the viscosity of the mold fluxes.

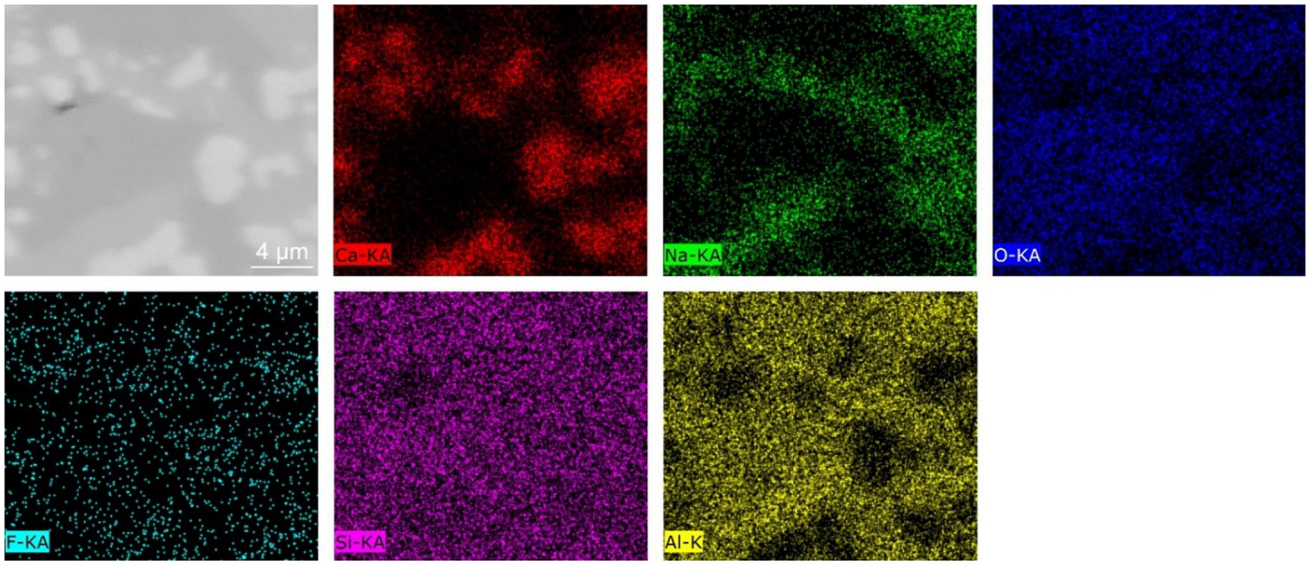

Fig. 12 Element mappings of crystals in slag D cooled at cooling rate of 10 °C/min

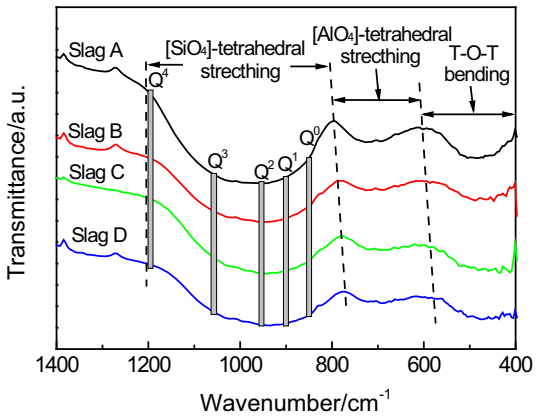

Fig. 13 FTIR spectroscopy of the mold fluxes

Table 2 Assignments of FTIR bands in spectra of studied mold fluxes

Wavenumber/cm^{-1}	Assignment	Refs.
400–600	T–O–T bending vibrations (T denotes Si, Al)	[18, 19]
600–800	$[AlO_4]$-tetrahedral stretching vibration	[20, 21]
800–1200	$[SiO_4]$-tetrahedral stretching vibration	[20, 22, 23]

4 Conclusions

1. The crystallization temperatures of the mold fluxes decreased with decreasing the SiO_2/Al_2O_3 ratio, and CaO/MnO_2 ratio has an opposite effect on the crystallization temperatures.
2. The crystalline phases precipitated in the mold flux were $Ca_4Si_2O_7F_2$ and $NaAlSiO_4$. Decreasing SiO_2/Al_2O_3 ratio and increasing CaO/MnO_2 ratio in the mold fluxes have no influence on the types of crystalline phases.
3. The dominant crystalline phase precipitated in each mold flux was $Ca_4Si_2O_7F_2$ with the dendritic morphology, except for part of that with globular morphology in the mold flux without MnO_2 addition. $NaAlSiO_4$ crystals are distributed in the space among $Ca_4Si_2O_7F_2$ crystals. The size of $Ca_4Si_2O_7F_2$ crystals in the mold flux with higher SiO_2/Al_2O_3 ratio is smaller than that in other mold fluxes, which is attributed to the higher polymerization degree of the mold flux with increasing SiO_2/Al_2O_3 ratio.
4. $[SiO_4]$-tetrahedral, $[AlO_4]$-tetrahedral and T–O–T bending depolymerized gradually with decreasing SiO_2/Al_2O_3 ratio, and an opposite trend was observed for the case with increasing CaO/MnO_2 ratio. The degree of polymerization of the mold fluxes decreased, which would result in the decrease in the viscosity of the mold fluxes.

Acknowledgements The financial support by the National Natural Science Foundation of China (Grant Nos. 51874026 and 51774225) and the Fundamental Research Funds for the Central Universities (Grant No. FRF-TP-18-004A3) is greatly acknowledged. The authors are thankful to the financial support from the State Key Laboratory of Advanced Metallurgy (Grant No. 41618020). This work was also partially financially supported by the National Key Research and Development Program of China (Grant No. 2016YFB0300604).

References

[1] S. Street, K. James, N. Minor, A. Roelant, J. Tremp, Iron Steel Technol. 5 (2008) 38–49.
[2] K. Blazek, H.B. Yin, G. Skoczylas, M. McClymonds, M. Frazee, Iron Steel Technol. 8 (2011) 231–240.
[3] W.L. Wang, K. Blazek, A. Cramb, Metall. Mater. Trans. B 39 (2008) 66–74.
[4] C.X. Ji, Y. Cui, Z. Zeng, Z.H. Tian, C.L. Zhao, G.S. Zhu, J. Iron Steel Res. Int. 22 (2015) Suppl. 1, 53–56.
[5] M.S. Kim, S.W. Lee, J.W. Cho, M.S. Park, H.G. Lee, Y.B. Kang, Metall. Mater. Trans. B 44 (2013) 299–308.
[6] J.W. Cho, K. Blazek, M. Frazee, H.B. Yin, J.H. Park, S.W. Moon, ISIJ Int. 53 (2013) 62–70.
[7] X.J. Fu, G.H. Wen, P. Tang, Q. Liu, Z.Y. Zhou, Ironmak. Steelmak. 41 (2014) 342–349.
[8] D. Xiao, W. Wang, B. Lu, Metall. Mater. Trans. B 46 (2015) 873–881.
[9] B. Lu, K. Chen, W. Wang, B. Jiang, Metall. Mater. Trans. B 45 (2014) 1496–1509.
[10] C.B. Shi, M.D. Seo, J.W. Cho, S.H. Kim, Metall. Mater. Trans. B 45 (2014) 1081–1097.
[11] L. Zhou, H. Li, W. Wang, Z. Wu, J. Yu, S. Xie, Metall. Mater. Trans. B 48 (2017) 2949–2960.
[12] X. Yu, G.H. Wen, P. Tang, B. Yang, J. Iron Steel Res. Int. 17 (2010) No. 5, 11–16.
[13] C.B. Shi, J. Li, J. W. Cho, F. Jiang, I. H. Jung, Metall. Mater. Trans. B 46 (2015) 2110–2120.
[14] J.L. Li, Q.F. Shu, X.M. Hou, K.C. Chou, ISIJ Int. 55 (2015) 830–836.
[15] H. Nakada, K. Nagata, ISIJ Int. 46 (2006) 441–449.
[16] M.D. Seo, C.B. Shi, J.W. Cho, S.H. Kim, Metall. Mater. Trans. B 45 (2014) 1874–1886.
[17] M.D. Seo, C.B. Shi, H. Wang, J.W. Cho, S.H. Kim, J. Non-Cryst. Solids 412 (2015) 58–65.
[18] H. Kim, W.H. Kim, I. Sohn, D.J. Min, Steel Res. Int. 81 (2010) 261–264.
[19] J.H. Park, D.J. Min, H.S. Song, Metall. Mater. Trans. B 35 (2004) 269–275.
[20] J.L. Liao, Y.Y. Zhang, S. Sridhar, X.D. Wang, Z.T. Zhang, ISIJ Int. 52 (2012) 753–758.
[21] G.H. Kim, C.S. Kim, I. Sohn, ISIJ Int. 53 (2013) 170–176.
[22] Z.J. Wang, Q.F. Shu, S. Sridhar, M. Zhang, M. Guo, Z.T. Zhang, Metall. Mater. Trans. B 46 (2015) 758–765.
[23] J.R. Kim, Y.S. Lee, D.J. Min, S.M. Jung, S.H. Yi, ISIJ Int. 44 (2004) 1291–1297.